JOURNAL OF AIRCRAFT
Vol. 47, No. 6, November–December 2010

Design Optimization of a Truss-Braced-Wing Transonic Transport Aircraft

Ohad Gur,* Manav Bhatia,* Joseph A. Schetz,† William H. Mason,‡ and Rakesh K. Kapania§
Virginia Polytechnic Institute and State University, Blacksburg, Virginia 24061-0203
and
Dimitri N. Mavris¶
Georgia Institute of Technology, Atlanta, Georgia 30332-0150

DOI: 10.2514/1.47546

This paper establishes the benefits of a truss-braced-wing transonic transport aircraft configuration compared to the cantilever-wing aircraft and to a strut-braced wing. Multidisciplinary design optimization is used to design aircraft with three wing configurations with increasing complexity of topology: cantilever, one-member truss (strut), and three-member truss. Three objective functions are studied: minimum takeoff gross weight, minimum fuel consumption and emissions, and maximum lift-to-drag ratio. A mission with a 7730 n mile range at a cruise Mach number of 0.85 is considered. The results show the significant advantage of strut and simple truss configurations over the conventional cantilever configuration. One comparison produces a reduction of 45% in the fuel consumption while decreasing the minimum takeoff gross weight by 15%. For a second comparison, the fuel weight is reduced by 33% with a decreased minimum takeoff gross weight of 19%. Very attractive vehicle performance can be achieved without the necessity of decreasing cruise Mach number. The results also indicate that a truss-braced wing has a greater potential for improved aerodynamic performance than other innovative aircraft configurations. Further studies will consider the inclusion of more complex truss topologies and other innovative technologies that are judged to be synergistic with truss-braced-wing configurations.

Nomenclature

AR	=	wing aspect ratio
b	=	wing span
C_L, C_D	=	lift and drag coefficient
$C_{L,\max}$	=	stall lift coefficient
C_l	=	two-dimensional lift coefficient
c	=	chord
c_{avg}	=	average wing chord
c_{CL}, c_{tip}	=	centerline and tip chord
F_s	=	shear force
H_{cr}	=	average cruise altitude
L/D	=	lift-to-drag ratio
Re_l	=	transition Reynolds number
S_w	=	wing area
$T_{\max}$	=	maximum required thrust
TF	=	laminar technology factor
TOGW	=	takeoff gross weight
t_{buckling}	=	thickness required to satisfy the buckling limit
t_{new}	=	updated skin-thickness value
t_{stress}	=	thickness required to satisfy the stress limit
t/c	=	thickness ratio
t/c_{CL}, t/c_{tip}	=	centerline and tip thickness-to-chord ratio
W_f	=	fuel weight, klb
W_{fold}	=	folding-wing-mechanism weight penalty
W_w	=	wing weight, klb
$\Lambda_{0.25}$	=	wing quarter-chord sweep angle, deg
η_{fold}	=	wing folding butt-line position to half-span ratio

Presented as Paper 2009-7114 at the 9th AIAA Aviation Technology, Integration, and Operations Conference (ATIO) and Aircraft Noise and Emissions Reduction Symposium (ANERS), Hilton Head, SC, 21–23 September 2009; received 6 Oct. 2009; revision received 2 August 2010; accepted for publication 15 August 2010.

*Research Associate, Aerospace and Ocean Engineering Department. Fellow AIAA.
†Holder of the Durham Chair, Aerospace and Ocean Engineering Department. Life Fellow AIAA.
‡Professor, Aerospace and Ocean Engineering Department. Associate Fellow AIAA.
§Mitchell Professor, Aerospace and Ocean Engineering Department. Associate Fellow AIAA.
¶Boeing Professor of Advanced Aerospace Systems Analysis and Director of Aerospace Systems Design Laboratory, Daniel Guggenheim School of Aerospace Engineering. Associate Fellow AIAA.

I. Introduction

TODAY, special attention is being paid to low-fuel-consumption and low-emissions air vehicles. This is due to an increasing environmental impact of air vehicles [1] and the need for energy independence. A possible option to tackle these problems is the use of exotic alternative propulsion systems such as all-electric emissionless vehicles [2]. Still, a large effort is being directed toward efficiency improvement of current airliners and the design of new, more efficient air vehicles.

One of the issues influencing the fuel consumption for a given vehicle mass, and thus also its emissions, is the vehicle drag, or lift-to-drag ratio. The different components of vehicle drag (e.g., induced, friction, profile, interference, and wave drag) are influenced by various aspects of the vehicle configuration. The wing span and the wing efficiency factor strongly influence the induced drag. The wing thickness-to-chord ratio t/c and the wing sweep angle affect both the wave (or compressibility) and friction drag. Green [3] reviewed some of these aspects while focusing on friction drag reduction using laminar flow control. Structural aspects for a conventional cantilever wing limit the potential reduction of thickness-to-chord ratio or an increase in wingspan due to the large weight penalty, thereby limiting performance improvements for a conventional cantilever-wing configuration.

During the 1950s Pfenninger [4] proposed the design of a truss-braced wing for transonic aircraft to achieve a reduction in the thickness-to-chord ratio and wing sweep (and an increase in wing span at a reduced structural weight) but with higher complexity, as shown in Fig. 1. Following Pfenninger's ideas, the concept of a strut-braced-wing (SBW) configuration was investigated using

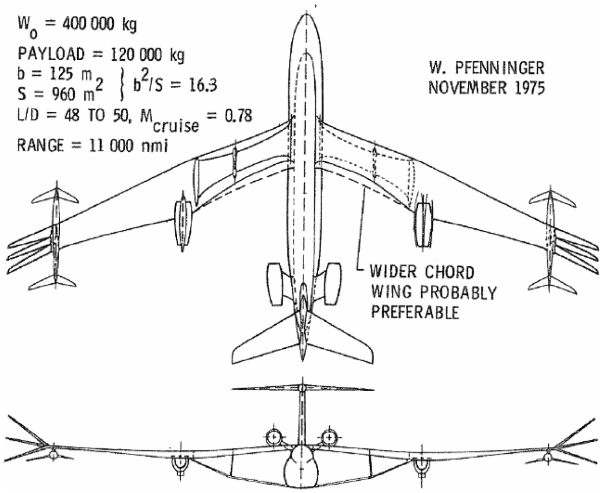

Fig. 1 One of Pfenninger's visions [4] for a truss-braced-wing aircraft.

multidisciplinary design optimization (MDO) tools [5–7]. These studies established the potential benefits of such configurations.

This paper extends the design domain to a multimember truss-braced-wing (TBW) configuration. To establish a consistent comparison, three different configurations are studied: a cantilever baseline, a single-member truss (henceforth called SBW), and a three-member jury-truss (henceforth called TBW) configuration. The paper includes a detailed description of the structural and aerodynamic models used within the MDO tool, and the resulting optimized configurations are presented along with conclusions highlighting the merits of a TBW configuration.

II. Problem Statement

The vehicle's mission is defined here as flying a range of 7730 n mile with 305 passengers, which is similar to that of the Boeing 777-200ER. Figure 2 shows the mission breakdown, which includes takeoff from an 11,000 ft runway, climb to an initial cruise altitude, and cruise for a range of 7730 n mile at constant Mach number of 0.85. The landing is done on an 11,000 ft field located at sea level with reserve fuel for an additional 350 n mile. Note that along the entire mission, a standard atmosphere is considered.

The optimization design problem can be described mathematically as a search process using a set of design variables that minimizes (or maximizes) a specific objective function that represents the design goal. This search process is carried out including numerous design constraints. What follows describes these three components: design goals, constraints, and design variables.

A. Design Goals

Various goals can be considered while designing an air vehicle [8,9], with an appropriate definition of the objective function for each goal. The current research focuses on three objective functions: minimum takeoff gross weight (TOGW), minimum fuel weight/emissions, and maximum lift-to-drag ratio L/D. These figures of merit represent different emphases.

The minimum-TOGW goal takes into account both fuel weight (which represents the operating cost) and vehicle empty weight (which represents the vehicle price). Thus, the minimum-TOGW objective function represents the life-cycle cost, and it is probably the most commonly used objective function for conceptual design.

The minimum-fuel objective function emphasizes lower operational cost and correlates to lower emissions. Thus, this objective function is referred to here as minimum fuel/emissions. Although this goal does not consider the initial capital cost of the vehicle, with the increasing fuel prices today and the importance of environmental issues, this objective function might be of considerable interest.

The maximum lift-to-drag-ratio objective function represents an aerodynamic goal, which determines the vehicle performance. Through the Breguet range equation it is easy to show how this figure of merit influences the vehicle range and thus may result in lower fuel consumption. However, maximizing the lift-to-drag ratio concentrates mostly on the aerodynamic properties of the vehicle, and its use as an objective function demonstrates the effect of concentrating on aerodynamic properties at the expense of the other disciplines.

The need for judicious comparison between the different design goals highlights the importance of engineering observations and their application in a subsequent design. This further reinforces the understanding that for real world problems MDO is not a man-out-of-the-loop process, but requires the judgment and creativity of an engineer.

B. Design Constraints

Most of the design constraints are imposed on performance, such as takeoff and landing field length, minimum rate of climb after takeoff, single-engine flight, etc. Additional constraints are imposed on maximum wingtip deflection while encountering a taxi bump and sufficient fuel capacity, as dictated by the mission.

The current design process includes the following constraints. These constraints are also listed in Table 1.

1) For the range constraint, the range of the vehicle using its full fuel capacity is not less than 7730 n mile with an additional 350 n mile reserve.

2) For the initial cruise rate-of-climb (ROC) constraint, the ROC at cruise flight conditions and initial cruise weight is higher than 300 ft/min.

3) For the maximum-C_l constraint, the local two-dimensional lift coefficient C_l at cruise flight conditions is no greater than 0.8. (This value represents a typical 2-D operating limit for transonic airfoils.)

4) For the fuel-capacity constraint, the available fuel volume in the main wing tanks and in the fuselage is higher than the required fuel for mission accomplishment. The fuselage is considered capable to carry up to 38,000 lb of fuel, the same as the 777-200ER.

5) For the wing-deflection constraint, at the taxi-bump condition, 2.0 g acceleration, the wing-system deflection does not exceed the ground clearance. The ground is considered to be located one fuselage diameter (20.3 ft) below the wing. The reason for using the fuselage diameter is that for the current study only high-wing configurations are considered. Note that the 2.0 g load case is used for the deflection constraint while the wing is structurally sized by a

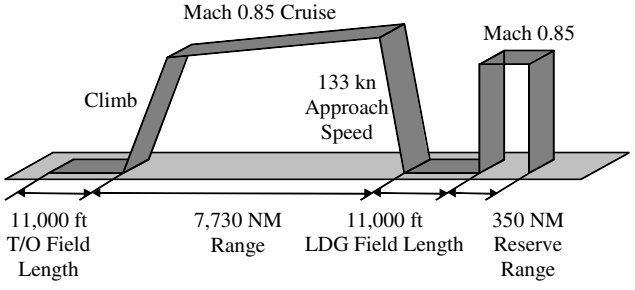

Fig. 2 Basic mission of the problem statement (T/O denotes takeoff and LDG denotes landing).

Table 1 Design constraints

Constraint	Value
Range	$\geq$ 7730 NM + 350 NM (reserve)
Initial cruise ROC	$\geq$ 300 ft/min
Maximum section C_l in cruise	$\leq$ 0.8
Available fuel volume	$\geq$ required fuel
Wingtip deflection	$\leq$ 20.3 ft
Second-segment climb gradient	$\geq$ 2.4%
Approach velocity	$\geq$ 132.5 knots true airspeed
Missed-approach climb gradient	$\geq$ 2.1%
Balanced-field length	$\leq$ 11,000 ft

Table 2 Design variables list

	Variable	Nomenclature	Cantilever	SBW	TBW
1	Wing CL section chord	c_1	√	√	√
2	Wing CL section thickness ratio	t/c_1	√	√	√
3	Break section Y coordinate	Y_2	√	√	√
4	Break section chord	c_2	√	√	√
5	Break section thickness ratio	t/c_2	√	√	√
6	Wingtip section X coordinate	X_3	√	√	√
7	Wingtip section Y coordinate	Y_3	√	√	√
8	Wingtip section chord	c_3	√	√	√
9	Wingtip section thickness ratio	t/c_3	√	√	√
10	Strut-CL section X coordinate	X_4	—	√	√
11	Strut-CL section chord	c_4	—	√	√
12	Strut-CL section thickness ratio	t/c_4	—	√	√
13	Strut-tip section Z coordinate	Z_5	—	√	√
14	Wing/jury intersection Y coordinate	Y_6	—	—	√
15	Strut/jury intersection Y coordinate	Y_7	—	—	√
16	Jury-down section chord	c_8	—	—	√
17	Jury-down section thickness ratio	t/c_8	—	—	√
18	Average cruise altitude	H_{cr}	√	√	√
19	Takeoff fuel weight	W_f	√	√	√
20	Maximum required thrust	T_{max}	√	√	√

set of 17 different load cases. These cases contain 2.5 g pulls and −1.0 g pushes along with the 2.0 g taxi bump (see Sec. III.A).

6) For the second-segment climb constraint, during takeoff at the second-segment conditions (1.2 × stall speed) the climb gradient should be higher than 2.4% [the requirement for a two-engine vehicle according to federal aviation regulations (FARs)].

7) For the approach-velocity constraint, during the approach condition ($C_L = 1.52$,** landing gear down) the vehicle can maintain true airspeed, which is less than 132.5 kt.

8) For the missed-approach constraint, during landing missed-approach conditions [$C_L = 1.52$ (see footnote **), landing gear up] the climb gradient should be higher than 2.1% (the requirement for a two-engine vehicle according to FARs).

9) For the balanced-field constraint, the takeoff and landing balanced-field length is less than 11,000 ft. The balanced-field constraint is calculated according to the Roskam model [10].

C. Design Variables

Design variables of the current TBW configuration contain the operational and geometric design variables listed in Table 2. The operational design variables define the performance potential of the vehicle and its ability to complete the required mission presented in Fig. 2. These are the average cruise altitude H_{cr}, takeoff fuel weight W_f, and maximum required thrust T_{max}.

The geometric design variables are defined according to prescribed cross sections (see Fig. 3). This geometric parameterization is described in detail in [11].

The geometric design variables are divided as follows:

1) Cantilever-wing design variables (total of nine) define a cantilever-wing geometry: the spanwise coordinates of the break and tip sections (Y_2 and Y_3, respectively); wingtip fuselage station X_3, which defines the wing sweep; centerline (CL), break, and tip chords (c_1, c_2, and c_3, respectively); and CL, break, and tip thickness ratios (t/c_1, t/c_2, and t/c_3, respectively).

2) SBW design variables (total of 13) define the SBW geometry. They include the nine cantilever design variables with an additional four variables: strut-CL body station X_4, which defines the strut sweep angle; strut-tip water line Z_5, which allows for an offset length; and †† strut-CL chord and thickness ratio, c_4 and t/c_4, respectively. Note that a constant chord and thickness are considered for the strut.

3) TBW design variables (total of 17) define the TBW configuration. This includes the 13 design variables of the SBW with the addition of four more design variables: the wing/jury intersection buttock line (BL), Y_6; strut/jury BL, Y_7; jury chord and thickness ratio, c_8, t/c_8, respectively.

The geometric design variables define the planform and geometry of the wing and truss members. The other geometry parameters remain constant throughout the design process: e.g., the vertical distance between the strut root and wing centerline. It is assumed that the aircraft has a fuselage similar to that of a Boeing 777. The tail is a fixed-size T-tail, and the engines are assumed to be fuselage-mounted. At this stage of the study an all-aluminum aircraft is assumed.

Note that the cantilever design is also assumed to be a high-wing configuration, thus enabling a true comparison to the SBW and TBW configurations.

III. MDO Framework and Methods

The MDO framework is composed of several analysis modules. A full and detailed description of this framework is given in [11]. Figure 4 shows the main elements of the framework. The main analyses (propulsion, aerodynamics, structures, and weight estimation) are located in a TOGW convergence loop that finds the TOGW for a specified set of design variables iteratively.

The calculation of the design goals and constraints is done as part of the outer optimization loop. For the current study, the optimization

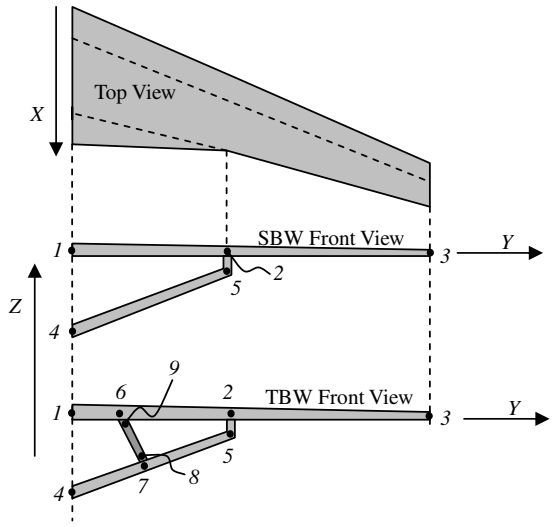

Fig. 3 Geometric design variables.

**This value represents 1.3 times the airspeed at stall conditions. A typical value for the stall lift coefficient, $C_{L,max} = 2.56$, is used.

††A vertical offset member was added to the wing/strut intersection to help reduce the interference drag [6,7].

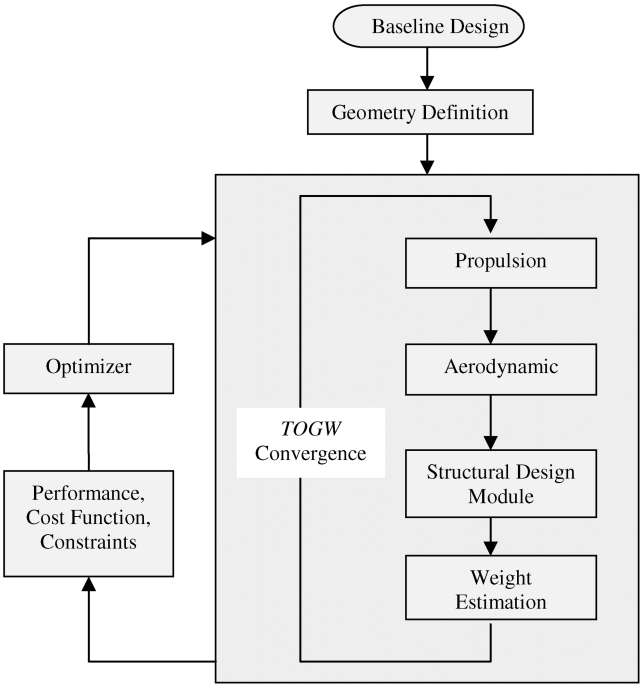

Fig. 4 TBW MDO design framework.

loop uses the Vanderplaats Research and Development DOT [12] modified-feasible-directions optimization algorithm scheme. One of the main weaknesses of a gradient-based optimization is the sensitivity of the final optimal design to the initial design variables and its inability to look beyond the nearest local minimum. Trying to avoid this, the optimization scheme is initiated from several different initial guesses, thus trying to find the global minimum. Although this method does not guarantee the global minimum, it strives to avoid any local minima.

The basic MDO approach is an extension of the approach used in earlier SBW method [7] using an updated design environment [11]. The three main modules in this MDO framework are: the structural design module, the aerodynamic analysis module, and the weight estimation module. In what follows, detailed descriptions of these modules are given.

A. Structural Design Module

For a given wing-truss geometric configuration, aerodynamic load, and fuel distribution, the structural module is used to calculate the minimum amount of material required such that the maximum stress in all structural members is below the specified material limit and that none of the structural members buckle under compressive force (that is, the buckling eigenvalue of each structural member is above unity). Note that the structural design module also uses the aerodynamic loading on the truss members; thus, the truss members experience bending.

The structural module is based on a combination of finite element analysis of the wing-truss configuration and the fully stressed design criteria. The structure is modeled as beam finite elements for the wing and truss members. Each element is idealized to be made up of only top and bottom wing skins and forward and rear webs (see Fig. 5). Although both rigid and joint intersections (e.g., wing and strut) are available, all intersections in the current effort are considered to be rigid.

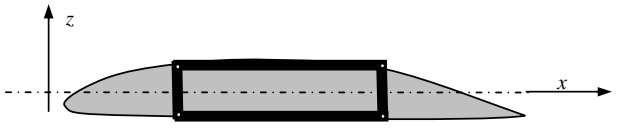

Fig. 5 Wing and truss-member cross sections are idealized to be made up of a torsion box.

The beam finite elements are formulated using Hermite interpolation functions [13]. The axial stiffness contribution is calculated using linear Lagrange interpolation functions for the nodal axial displacements. The resulting structural finite element stiffness matrix is used to calculate the displacements and stresses. The material properties assumed for the current study are given in Table 3. A safety factor of 1.5 is used for each load case, and the total loading is a combination of the aerodynamic lift, fuel inertia loads, and self-weight inertia of the structural elements.

A total of 17 load cases are considered for structural sizing: 1) +2.5 g pull-up maneuver at 0 and 100% fuel, 2) −1.0 *g* pull-up maneuver at 0 and 100% fuel, 3) 2 *g* taxi bump at 100% fuel (does not include aerodynamic lift); 4) six gust load cases with 0% fuel and FAR discrete vertical gusts specified at different altitudes: 0, 10, 20, 30, and 40 kft; and 5) six gust load cases with 100% fuel and FAR discrete vertical gusts specified at different altitudes: 0, 10, 20, 30, and 40 kft.

The first two static loadings are considered to be representative for maximum positive and negative load factors of transport air vehicles. The 2 *g* taxi bump represents harsh ground handling, and it is also used for the wing deflection constraint. For the current level of fidelity the 2 *g* taxi bump is considered as an equivalent static load case, rather than as a structural dynamic response.

Because of the low wing loading, the gust load cases are considered to be important; thus, several cases at a wide range of flight conditions are used. The gust loading cases are derived from a simple one-degree-of-freedom representation [11,15] and are calculated in the aerodynamic analysis module.

Note that some additional load cases could also be considered, such as hard landing. Still, these 17 load cases represent a typical set for structural sizing.

Sizing the skin- and web-thickness values for a given wing and truss geometry (chord t/c ratio) uses two criteria: maximum yield stress and buckling-load factor. The Euler buckling approximation is used for the buckling loads. Thus, after each fully stressed design iteration, the new thickness values t_{new} are set to

$$t_{\text{new}} = \max(t_{\text{stress}}, t_{\text{buckling}}) \tag{1}$$

where t_{stress} is the thickness required to satisfy the stress limit of the element, and t_{buckling} is the thickness required to satisfy the buckling limit of the member. This iteration is performed until convergence on the wing mass is obtained. Because of the low analysis cost, a high number of structural members (one element per 3 ft of structural length) are used in this modeling approach, and one thickness value is defined for each structural finite element.

It is important to note that the fully stressed design approach dictates that each element be sized so that it carries the maximum allowable stress. Hence, this approach cannot be used to satisfy a displacement constraint if the design process involves only structural sizing. The current MDO study involves shape optimization in addition to sizing using the fully stressed design approach. A constraint is imposed on the wing displacement, for which the calculated displacement values are returned to the optimizer, since it cannot be handled by the structural design routine. The shape optimizer then changes the shape design parameters (listed in Table 2) to meet the displacement constraint.

The structural sizing approach described in this section results in a bilevel optimization architecture, where the upper-level optimizer handles all the geometric design variables, and the lower-level optimal design routine (working within the structural module)

Table 3 Aluminum material (Al-7075 [14]) properties assumed for current study

Material property	Value
Young's modulus	1.5×10^9 psf
Poisson ratio	0.33
Density	178.29 lb/ft^3
Max allowable stress	8.01×10^6 psf

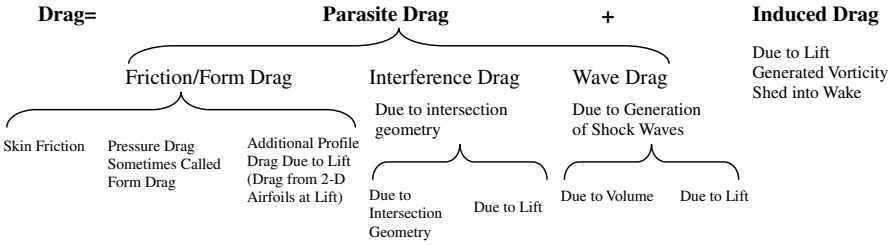

Fig. 6 Drag breakdown.

calculates the minimum structural mass and the resulting deflections for the specified aerodynamic loading. The module calculates the bending and shear mass of the wing system. The other components of the wing-system mass (mainly secondary structure) are added using the flight optimization system (FLOPS) developed by NASA [16] (see Sec. III.C.).

The MDO results presented in this paper are based on a quasi-steady structural analysis neglecting aeroelastic coupling; that is, the influence of wing flexibility on aerodynamic loads is neglected during calculation of the structural mass. Wing flutter is also an important structural dynamics consideration. Ongoing MDO studies [17] aim to use a combination of structural tailoring and active flutter suppression techniques to achieve the required aeroelastic performance.

B. Aerodynamic Analysis and Design Modules

The aerodynamic analysis calculates the optimum wing loading for a given geometry using a Trefftz plane analysis [18,19]. The spanwise loading is also calculated for the truss members; thus, the analysis predicts the ideal lift distribution in order to maximize the aerodynamic benefit of this nonplanar configuration. Note that this benefit is less than a biplane configuration due to the low clearance between the strut and the wing.

In addition to the optimal spanwise lift distribution, this analysis also computes the minimum induced drag. This is combined with the friction, form, wave, and interference drag to define the total drag of the vehicle configuration. This drag breakdown is presented in Fig. 6 and thoroughly described in [20]. In what follows, a short summary of this breakdown is presented.

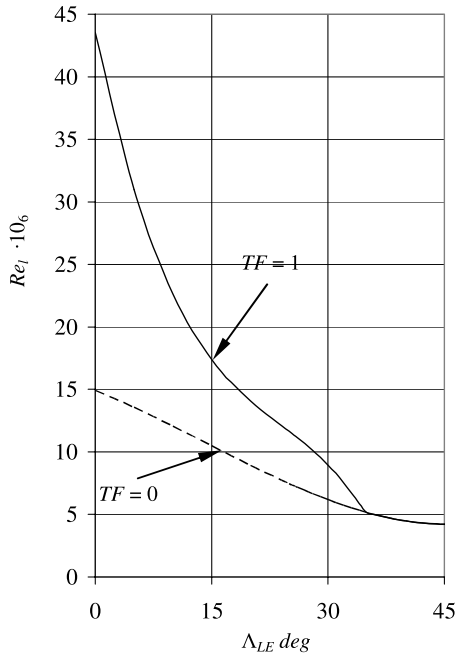

Fig. 7 Wing transition Reynolds number and technology-factor definition.

The friction/form drag calculation is based on the wetted area and uses predictions of skin-friction models and form-factor estimations. The skin-friction prediction uses laminar and turbulent boundary-layer models. For laminar flow, the Eckert reference-temperature method [21] is used, and for turbulent flow, the Van Driest II method [22,23] (based on the von Kármán–Schoenherr model) is used. The total skin-friction coefficient is based on a composition of the laminar/turbulent flow. Several composition formulas are available [24,25], and for the current research, Schlichting's composition formula is used [26]. The complete model for the flat-plate skin-friction coefficient is available online.[‡‡]

The results presented in this paper are based on two different laminar/turbulent transition criteria: one representing the state of technology in present-day airliners (denoted here as *current technology*, technology factor TF = 0) and the other representing potential improvements in wing surface airflow, using natural laminar flow, by the year 2035 (denoted here as *aggressive technology*, technology factor TF = 1). This simple approach is used to determine the chordwise location of boundary-layer transition. Figure 7 presents two curves of transition Reynolds number based on the chordwise Reynolds number Re_l (taken from [27]). The dashed curve designated as TF = 0 (technology factor of 0) is for natural laminar flow on standard wings [28]. The solid curve, designated as TF = 1, refers to natural laminar flow airfoils [29]. In all cases here, laminar flow is limited to 70% of the wing chord.

The flat-plate equivalent transition Reynolds number on the fuselage is considered to be 2.5×10^6. Note that at cruise conditions the value of 2.5×10^6 is equivalent to about 1.5 ft, which for a 206 ft fuselage means practically a fully turbulent fuselage. For the current research, riblets are used for the aggressive-technology cases; thus, the turbulent friction coefficient for the fuselage is assumed to be decreased by a conservative value of 5%.

A form factor is used to represent the drag correction due to both thickness and pressure drag, which is sometimes referred to as profile drag. Many form-factor models exist [30–35], and the current study uses the Grumman lifting-surface form factor $\mathrm{FF}_{\mathrm{Wing}}$ for the wing, truss members, and tail:

$$\mathrm{FF}_{\mathrm{Wing}} = 1 + 1.8\frac{t}{c} + 50\left(\frac{t}{c}\right)^4 \tag{2}$$

where t/c is the maximum cross-sectional thickness ratio.

The Hoerner [30] body-of-revolution form factor $\mathrm{FF}_{\mathrm{Body}}$ is used for the fuselage and nacelles:

$$\mathrm{FF}_{\mathrm{Body}} = 1 + \frac{1.5}{(l/d)^{1.5}} + \frac{7}{(l/d)^3} \tag{3}$$

where l/d is the body fineness ratio.

The wave drag is a result of the shock waves created over the vehicle; thus, it becomes important at high subsonic speeds. The wave drag model used here is based on the Korn equation extended to swept wings [36] with a Korn factor of 0.95, implying the use of supercritical airfoils. Along with Lock's fourth power law [37–39], the drag rise, critical Mach number, and drag-divergence Mach

[‡‡]Data available online at http://www.aoe.vt.edu/~mason/Mason_f/FRICTman.pdf [retrieved 1 September 2010].

number can be estimated. For the aggressive-technology case, a highly supercritical airfoil is used: namely, a Korn factor of 0.95. The current-technology case uses a Korn factor of 0.91, which represents the current 777 airfoil technology.

Note that the treatment of all lifting or truss-member surfaces is the same. Thus, the main wing, truss members, horizontal tail, and vertical tail are treated with the same models for induced, friction/form, and wave drag.

Interference drag results from the airflow over the intersection of a lifting or truss-member surface with either the fuselage or with another lifting surface. The fuselage/wing and truss/wing interference drag are modeled using methods given by Hoerner [30] and precomputed drag response-surface models obtained from viscous computational fluid dynamics (CFD) simulations [40]. The truss/strut intersections share similar chord lengths; thus, the interference drag is based on drag response surfaces obtained from viscous CFD simulations of two similar chord/wing intersections [41].

Note that these interference drag models do not include any fairing effects. According to the literature a fairing is able to reduce the interference drag by at least by 90% (a factor of 0.1 times the unfaired drag estimate) [30] and in certain cases even to make the interference drag negligible [33,35,42]. This suggests that for the current-technology case a conventional fairing factor of 0.1 should be used, and for the aggressive-technology case an aggressive fairing factor of 0.02 should be used.

C. Weight Estimation Module

As stated before, the wing bending and shear-material weights are calculated using the structural design module. This weight is then supplemented using FLOPS [16] formulas taking into account the other wing components (flaps, actuators, etc.). The FLOPS secondary weight correction is used just for the main wing. The other wing-system component weights are taken straight from the structural design module.

Figure 8 presents comparison between the Shevell [33] wing-weight index regression line and the current weight-estimation methods. The vertical axis is the wing loading, and the horizontal axis is the wing-weight index, which represents the wing geometric properties and the structural loading parameters. The solid line is taken from Shevell [33] (p. 392) and was substantiated using various air-vehicle data (e.g., DC-8, DC-9, DC-10, 707, and 727). Two different sets of data points appear on the figure. The first set is the load-bearing material weight as calculated using the current structural design module. The other set of data points is the total estimated wing weight after adding the FLOPS additional weight estimation. Most of the vehicles calculated using the current module show good comparison with the Shevell line. One exception is the 777 data point, which represents a more advanced vehicle compared to the other vehicles. Still, this comparison validates the current structural weight estimation.

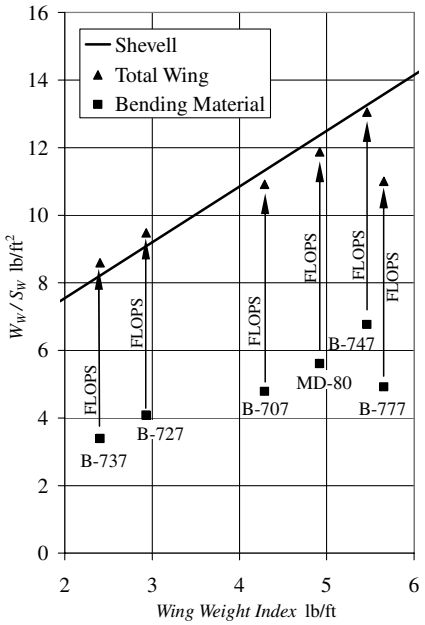

Fig. 8 Comparison of Shevell [33] wing-weight data and current wing-weight-estimation method.

Note that this validation uses just cantilever configurations. The authors are not aware of any similar available data for TBW configurations. Hence, we use the FLOPS corrections based on the structural mass calculated by our analysis and design module.

The remaining components (fuselage, empennage, etc.) weight estimations are done using FLOPS. Two weight penalties are then added to the FLOPS weight estimation: a folding-mechanism weight penalty and a fuselage weight penalty due to pressurization influence.

The folding-wing mechanism is used to allow spans higher than the 80 m (262 ft) gate-box limit. Thus, it is only used for configurations with spans over 80 m. Based on an elliptic loading distribution, the shear force F_s acting at the folding butt line is defined as

$$\frac{F_s}{\text{TOGW}} = \frac{1}{2}\cdot\left(1 - \frac{2}{\pi}\cdot\eta_{\text{fold}}\cdot\sqrt{1-\eta_{\text{fold}}^2} - \frac{2}{\pi}\cdot\sin^{-1}\eta_{\text{fold}}\right) \quad (4)$$

where η_{fold} is the folding position butt line to half-span ratio.

Using Eq. (4) and based on the 3000 lb penalty of the 21 ft wingtip folding mechanism of the Boeing 777 [43], the estimated weight penalty of the folding mechanism, W_{fold}, can be found:

$$\frac{W_{\text{fold}}}{\text{TOGW}} = 0.07\cdot\frac{F_s}{\text{TOGW}} \quad (5)$$

Note that this model assumes that the weight penalty is proportional to the shear force acting on the folding mechanism. Two different folding-mechanism weight-penalty models for fighter aircraft are available by York and Labell [44] and by Raymer [35]. For 777 data, Eq. (5) gives a weight penalty of 3000 lb, the York and Labell [44] model gives 3130 lb, and the Raymer [35] model gives 3040 lb.

The fuselage weight estimation is based on FLOPS. Many of the resulting configurations in the current studies reach high cruise altitudes, up to 48,000 ft. This cruise altitude required a heavier fuselage, due to the higher pressure differences between the cabin and the surrounding atmosphere. A model described in Torenbeek [31] is used to modify the FLOPS calculation.

IV. Results

Using the MDO methods described in the preceding sections, results for the following combination of cases are presented: 1) three configurations: cantilever, single-member strut (SBW), and jury truss (TBW); 2) three design objective functions: minimum TOGW, minimum fuel weight/emissions, and maximum L/D; and 3) two drag cases: aggressive technology (TF = 1, Korn factor of 0.95, and fairing factor of 0.02) and current technology (TF = 0, Korn factor of 0.91, and fairing factor of 0.1).

This makes a total number of 18 design cases. Figure 9 shows visualizations of nine of these designs for the aggressive-technology case. Note that the drawings are to scale. Tables 4–6 present a selection of the numerical results for the three objective function cases.

Much additional information is also found during the calculations. Note that for each case, the variable that represents the objective function comes out as the best. For example, the smallest TOGW was achieved when the TOGW is used as a cost function. This gives some confidence in the design process.

The current-technology cantilever minimum TOGW is representative of current airliners. The reported 777 TOGW and fuel weight, for a 7730 n mile mission, are 656 klb and 290 klb, respectively. These values can be compared with the somewhat lower values for current-technology cantilever minimum-TOGW design here. Note that the Boeing 777 was not optimized for minimum

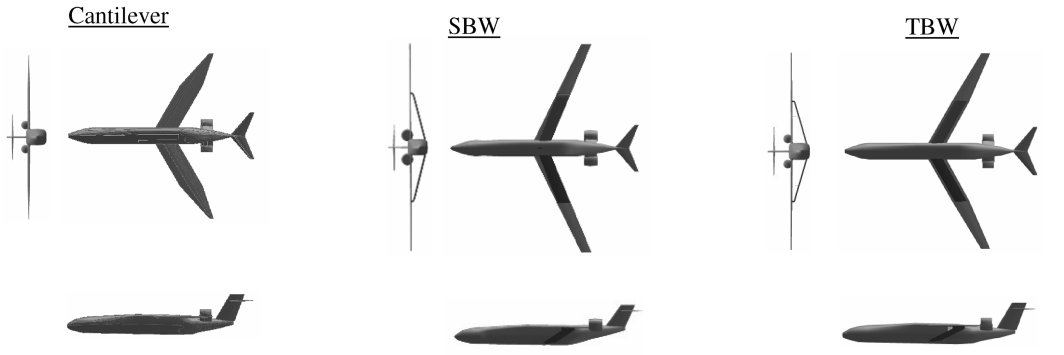

a) Minimum TOGW, *Aggressive Technology*

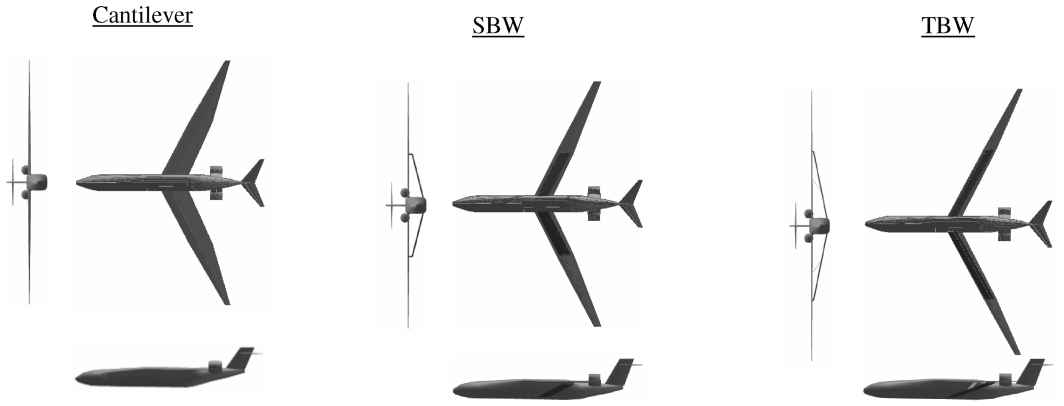

b) Minimum Fuel/Emissions, *Aggressive Technology*

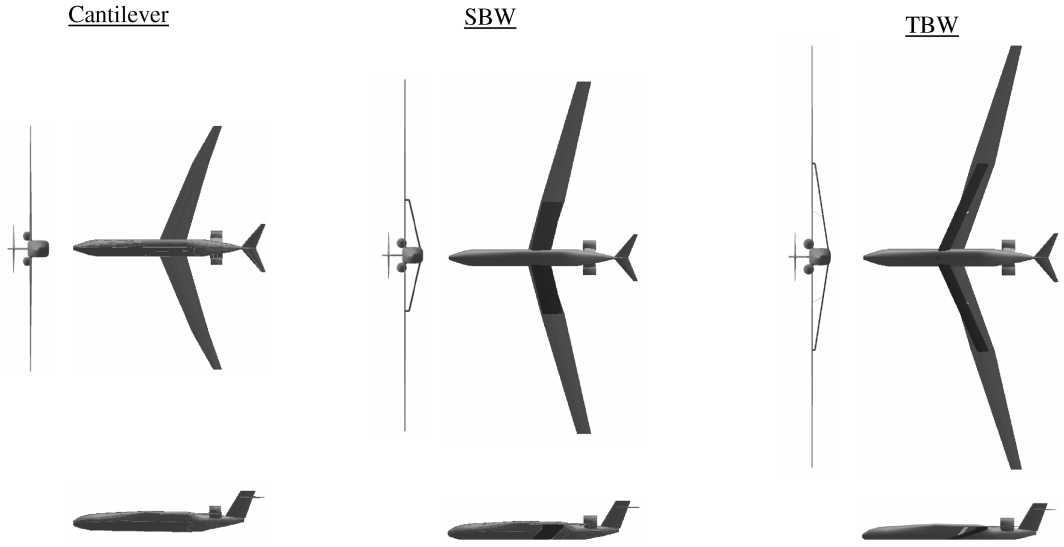

c) Maximum L/D, *Aggressive Technology*

Fig. 9 Optimal design configurations for aggressive-technology cases.

TOGW, for a single mission, and it was built with the intention of future growth.

To understand the trends of the results, it is important to keep in mind that the primary influence of adding a supporting truss to a wing structure is to achieve lower spanwise bending moments for a given loading. This results in a lighter wing structure and allows the span to increase, the section thickness to decrease, and the chord to decrease.

The higher wingspan also results in long and slender truss members with buckling-load capacity approximately inversely proportional to the square of member length. This is more critical for the SBW design than for the TBW, since the support members tend to be shorter for the TBW. The thin and slender wing holds less fuel; thus, a fuselage fuel tank is used.

Aerodynamically, most of the design trends help in reducing drag. The high aspect ratio reduces the induced drag, while the low thickness decreases the wave and form drag. Shorter chords allow more laminar flow. Unsweeping of the wing increases the chordwise length of laminar flow, due to higher transition Reynolds number (Fig. 7); thus, the friction drag is decreased. On the other hand, unsweeping has an adverse influence on the wave drag. The final sweep angle represents a balance between these two trends. Generally, adding truss members reduces the drag thereby increasing lift-to-drag ratio and decreasing the fuel weight requirement.

Table 4 Optimal design configurations for minimum-TOGW objective function

	TOGW, klb	W_w, klb	W_f, klb	L/D	$b/2$, ft	S_w, kft^2	c_{avg}, ft	AR	H_{cr}, kft	W/S_w, psf	$\Lambda_{0.25,\text{wing}}$, deg	t/c_{CL}, %	t/c_{tip}, %	t_{CL}, ft	t_{tip}, ft	c_{CL}, ft	c_{tip}, ft
Cantilever																	
Current technology	593	83	238	20	105	5.0	24	9	37	118	37	11.8	11.4	3.4	0.7	29	9
Aggressive technology	522	70	186	24	100	4.8	23	9	40	109	33	11.9	11.4	3.3	0.6	28	5
SBW																	
Current technology	579	88	216	22	120	5.4	23	11	42	107	33	9.1	6.2	2.5	0.8	28	13
Aggressive technology	491	65	161	26	120	4.5	19	13	45	108	29	9.7	10.3	2.2	1.2	22	12
TBW																	
Current technology	549	69	208	21	112	4.6	21	11	42	118	36	9.7	10.3	2.3	1.1	24	10
Aggressive technology	481	59	160	26	115	4.3	18	13	45	111	29	9.7	10.3	2.1	1.1	22	11

Table 5 Optimal design configurations for minimum-fuel/emissions objective function

	TOGW, klb	W_w, klb	W_f, klb	L/D	$b/2$, ft	S_w, kft^2	c_{avg}, ft	AR	H_{cr}, kft	W/S_w, psf	$\Lambda_{0.25,\text{wing}}$, deg	t/c_{CL}, %	t/c_{tip}, %	t_{CL}, ft	t_{tip}, ft	c_{CL}, ft	c_{tip}, ft
Cantilever																	
Current technology	606	118	204	25	135	7.2	27	10	46	84	33	9.4	6.4	3.3	0.3	35	5
Aggressive technology	563	126	160	31	150	7.3	24	12	48	77	27	10.3	6.5	3.5	0.4	34	6
SBW																	
Current technology	591	114	196	25	140	5.7	21	14	47	103	33	7.7	5.9	1.9	0.4	26	6
Aggressive technology	532	112	149	32	150	5.4	18	16	48	100	26	6.4	6.1	1.5	0.5	23	9
TBW																	
Current technology	568	101	186	25	150	5.2	17	18	48	108	34	8.7	7.8	1.9	0.5	21	6
Aggressive technology	503	102	131	36	165	4.7	14	23	48	106	28	8.8	7.8	1.6	0.5	18	6

Table 6 Optimal design configurations for maximum-L/D objective function

	TOGW, klb	W_w, klb	W_f, klb	L/D	$b/2$, ft	S_w, kft^2	c_{avg}, ft	AR	H_{cr}, kft	W/S_w, psf	$\Lambda_{0.25,\text{wing}}$, deg	t/c_{CL}, %	t/c_{tip}, %	t_{CL}, ft	t_{tip}, ft	c_{CL}, ft	c_{tip}, ft
Cantilever																	
Current technology	757	199	262	26	140	7.2	26	11	43	105	28	6.3	5.0	2.7	0.4	43	8
Aggressive technology	595	151	171	32	145	6.7	23	13	45	89	23	8.1	7.6	2.7	0.8	33	10
SBW																	
Current technology	1007	381	304	30	210	10.1	24	17	46	99	27	6.5	5.3	2.3	0.3	35	5
Aggressive technology	840	341	201	40	215	10.3	24	18	48	81	15	5.0	5.0	1.2	0.9	24	17
TBW																	
Current technology	962	378	266	33	240	11.1	23	21	48	86	25	5.0	5.0	1.3	0.4	26	8
Aggressive technology	953	446	200	48	250	11.1	22	23	48	86	17	5.0	5.0	1.0	0.6	21	13

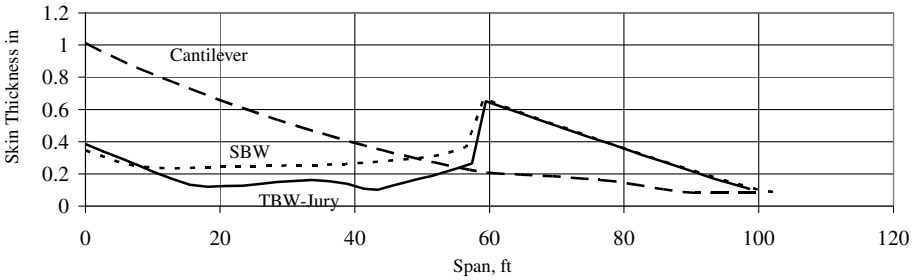

a) Minimum *TOGW, Aggressive Technology*

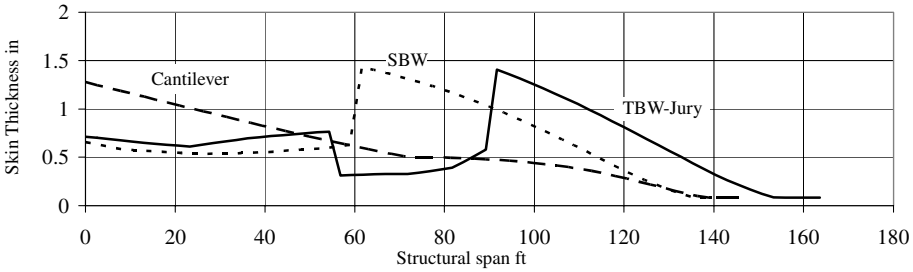

b) Minimum Fuel/Emissions, *Aggressive Technology*

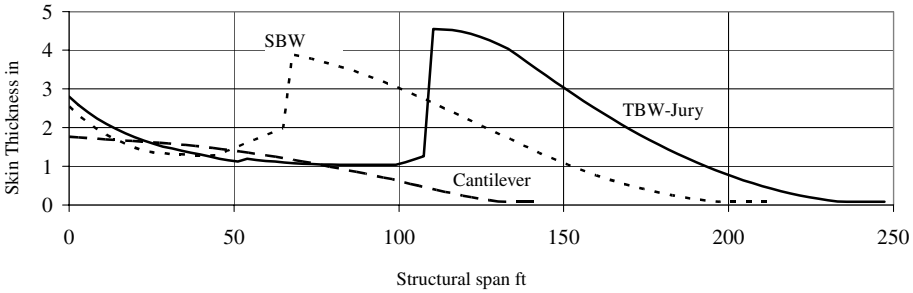

c) Maximum L/D, *Aggressive Technology*

Fig. 10 Skin-thickness plot for three different objective-function designs and aggressive-technology cases.

For the cases of minimum-TOGW objective function (Table 4), both the SBW and TBW configurations exhibit lower wing weight for similar span and AR. This can also be seen in the wing skin-thickness plot (Fig. 10a). It is noticeable that the presence of a truss considerably lowers the skin thickness in the inboard part of the wing and thus lowers the wing weight.

For the cases of the minimum-fuel/emissions objective function (Table 5 and Fig. 10b), the increased span and AR of the SBW and TBW configurations increase the lift-to-drag ratio L/D by reducing the induced drag. In addition, the increased wing area together with the higher cruise altitude decreases the zero-lift drag coefficient. This results in a lower fuel weight, along with lower TOGW.

For the maximum-L/D objective-function cases (Table 6 and Fig. 10c) the spans reach up to 250 ft with AR up to 23. Similar to the minimum-fuel/emissions cases, this trend allows very high $L/D \approx 48$. Still, the fuel weight is higher than in the previous case. This is due to the high wing weight that results in high TOGW.

The L/D values for the optimized minimum-fuel designs (36) and maximum L/D (48) are more than double that of the current generation commercial airliners (e.g., for the Boeing 777 $L/D \sim 20$). These high L/D ratios are characterized by high spans and ARs.

The difference between the two drag models (aggressive technology and current technology) is about 15% of the TOGW in the case of the minimum-TOGW objective function (Table 4). It reaches about 10% of fuel weight for the minimum-fuel-weight objective-function case (Table 5) and is 25% of L/D for the maximum-L/D objective-function case.

Considering a comparison between the TBW and SBW configurations, the addition of a truss member has a small influence on the minimum-TOGW designs (Table 4), but lowers the fuel weight by about 10% for the minimum-fuel-weight objective function (Table 5). For the maximum-L/D objective function, adding a truss member increases the L/D by 20%.

Numerous additional comparisons can be made, however; two we found of interest are current-technology cantilever minimum-TOGW versus aggressive-technology TBW minimum-fuel-weight designs and current-technology cantilever minimum-TOGW versus aggressive-technology TBW minimum-TOGW designs.

1) For current-technology cantilever minimum-TOGW versus aggressive-technology TBW minimum-fuel-weight designs, comparing the current-technology cantilever minimum-TOGW design with the aggressive-technology TBW minimum-fuel-weight design shows that the latter achieves a decrease of 15% TOGW (90 klb) and requires 45% less fuel weight (107 klb), which exhibits the important potential of this configuration. This reduction in fuel weight is partially achieved by a higher span (half-span of 165 ft versus 105 ft), which also results in a heavier wing structural weight.

2) For current-technology cantilever minimum-TOGW versus aggressive-technology TBW minimum-TOGW designs, the latter design shows a decrease of 78 klb (33%) fuel weight along with

119 klb (19%) of the TOGW and 24 klb (29%) reduction of the structural weight. This implies that both life-cycle cost (represented by the TOGW) and operating cost (represented by the fuel weight) are significantly decreased.

V. Conclusions

The conceptual design of a simple truss-braced-wing transonic transport aircraft configuration was presented. The design process uses an MDO framework, which includes structural design, aerodynamic analysis, and design, and weight-estimation modules along with other components (optimizer, propulsion module, etc.).

The MDO results used three different objective functions (minimum TOGW, minimum fuel/emissions, and maximum lift-to-drag ratio), three basic configurations (cantilever, SBW, Jury-TBW), and two aerodynamic models. The results prove that adding truss members enables an increased wing span and thus lowers induced drag. In addition, the wing thickness and chord decrease along with friction and wave drag components. These trends occur due to improved structural behavior. Thus, for the same weight, higher aspect ratios and lower section thicknesses are possible.

For the case of the minimum-TOGW objective function, the SBW and TBW configurations have a lower wing weight with higher span and AR as compared to the cantilever-wing baseline configuration. The minimum-fuel/emissions and the maximum-L/D objective functions exhibit higher spans and higher lift-to-drag ratios (36 for minimum fuel/emissions, and 48 for the maximum L/D).

The influence of the two aerodynamic models (aggressive technology and current technology) is 10–25% of the vehicles' performance, depending on the objective function considered. The comparison between the TBW and SBW configurations shows a difference of about 10–20%, again depending on the objective function considered.

Cross-comparisons between different objective functions reveal the high potential for the TBW configuration compared to the current-technology cantilever-wing configuration. One comparison produced a reduction of 45% in the fuel consumption while decreasing the TOGW by 15%. For a second comparison the fuel weight is reduced by 33% with a decreased TOGW of 19%.

The main feature of the TBW configurations is the high-AR wings with lower section thickness and chord, which raises a possible concern with the vehicle aeroelastic characteristics. A preliminary study of the flutter performance of these configurations was conducted. The analysis was performed using two separate models of the entire wing system. All wing and truss members were included in both the aerodynamic and structural model for a flutter analysis. The aerodynamic model calculated the unsteady forces on the wing and the truss members and similarly, the structural model calculated the normal modes including the truss members. The first flutter model was created and analyzed in NASTRAN using the doublet-lattice method for unsteady aerodynamics, and a three-dimensional shell model of the wing-box. The second flutter model used a three-dimensional beam idealization of the wing and the truss assembly with strip-theory-based unsteady aerodynamics. For the sake of brevity, only the important conclusion of this study is presented here and the details of the aeroelastic analysis will be presented in a following paper. It is important to note that flutter analyses of the MDO configurations predicts that none of the SBW and TBW configurations designed for either the minimum-TOGW or minimum-fuel/emissions objective functions experience flutter within the flight envelope. The configurations designed for maximum-L/D objective function have very large spans and have low flutter speeds. However, parametric aeroelastic studies [17] have shown that a significant potential exists for structural tailoring with the number and relative orientation of the wing and truss members. A more detailed discussion of the flutter study will be published in future papers. The results presented in this paper demonstrate that the TBW configuration has a high potential for more efficient future vehicles. It also indicates that a truss-braced wing has a greater potential for improved aerodynamic performance than has been reported for other innovative aircraft configurations. However, there is much more work that needs to be done. First, more complex truss technologies need to be considered. The use of truss topology optimization methods will be thoroughly explored in the rich parameter space. Second, the aeroelastic studies have to be expanded and those important effects must be included within the MDO framework. Third, methods for reducing the drag of the fuselage, and perhaps the tail, must be aggressively pursued. The current optimized designs do not yet represent *balanced* designs. The drag of the wings has been decreased, but the fuselage drag was not decreased other than by adding riblets. The MDO addressed the resulting situation by increasing the cruise altitude. Benefits of imbedding the engines in the fuselage employing boundary-layer ingestion inlets will be explored, likely following the suggestions of Goldschmied [45]. This has the potential of reducing the net drag of the fuselage by 30–50%. In addition, adding thrust vector control to the exhaust nozzle might permit elimination of the tail. Circulation control is attractive for this application. Implementation of these steps will permit us to more fully show the real potential of truss-braced-wing configurations for transonic transport aircraft.

Acknowledgments

The authors would like to acknowledge the financial support of NASA Langley Research Center with Vivek Mukhopadhyay as Technical Monitor. Dennis Bushnell inspired our efforts. Bernard Grossman of the National Institute for Aerospace, Raphael T. Haftka of the University of Florida, George Inger of Virginia Polytechnical Institute and State University, Taewoo Nam and Hongjun Ran of Georgia Institute of Technology, and Rosa Avalos from Virginia Polytechnic Institute and State University all contributed to this work.

References

[1] Takeda, K., Takeda, A. L., Bryant, J., and Clegg, A. J., "Systematic Review of the Impact of Emissions from Aviation on Current and Future Climate," *The Aeronautical Journal*, Vol. 112, No. 1135, Sept. 2008, pp. 493–522.

[2] Alexander, D., Lee, Y-M., Guynn, M., and Bushnell, D., "Emissionless Aircraft Study," 38th AIAA/ASME/SAE/ASEE Joint Propulsion Conference and Exhibit, AIAA Paper 2002-4056, Indianapolis, IN, July 2002.

[3] Green, J. E., "Laminar Flow Control—Back to the Future?," 38th Fluid Dynamics Conference and Exhibit, AIAA Paper 2008-3738, Seattle, WA, June 2008.

[4] Pfenninger, W., "Laminar Flow Control Laminarization," AGARD Rept. 654, Neully-sur-Seine, France, 1977.

[5] Grasmeyer, J. M., "Multidisciplinary Design Optimization of a Transonic Strut-Braced Wing Aircraft," 37th AIAA Aerospace Sciences Meeting and Exhibit, AIAA Paper 1999-0010, Reno, NV, Jan. 1999.

[6] Gundlach, J. F. IV., Tétrault, P.-A., Gern, F. H., Nagshineh-Pour, A. H., Ko A. Y-Y., Schetz, J. A., Mason, W. H., Kapania, R. K., Grossman, B., and Haftka, R. T., "Conceptual Design Studies of a Strut-Braced Wing Transonic Transport," *Journal of Aircraft*, Vol. 37, No. 6, Nov.–Dec. 2000, pp. 976–983. doi:10.2514/2.2724

[7] Gern, F. H., Ko, A. Y-Y., Grossman, B., Haftka, R. T., Kapania, R. K., Mason, W. H., and Schetz, J. A., "Transport Weight Reduction Through MDO: The Strut-Braced Wing Transonic Transport," 35th AIAA Fluid Dynamics Conference and Exhibit, AIAA Paper 2005-4667, Toronto, Ontario, June 2005.

[8] Jensen, S. C., Rettie, I. H., and Barber, E. A., "Role of Figure of Merit in Design Optimization and Technology Assessment," *Journal of Aircraft*, Vol. 18, No. 2, 1981, pp. 76–81. doi:10.2514/3.57468

[9] Malone, B., and Mason, W. H., "Aircraft Concept Optimization Using Parametric Multiobjective Figures of Merit," *Journal of Aircraft*, Vol. 33, No. 2, 1996, pp. 444–445. doi:10.2514/3.46960

[10] Lan, C-T. E., and Roskam, J., *Airplane Aerodynamics and Performance*, Roskam Aviation and Engineering Corp., Lawrence, KS, 1988.

[11] Gur, O., Bhatia, M., Mason, W. H., Schetz, J. A., Kapania, R. K., and Nam, T., "Development of Framework for Truss-Braced Wing Conceptual MDO," 6th AIAA Multidisciplinary Design Optimization Specialist Conference, AIAA Paper 2010-2754, Orlando, FL,

April 2010.
[12] DOT, Design Optimization Tools, Software Package, Ver. 5.0, Vanderplaats Research and Development, Inc., Colorado Springs, CO, Jan. 1999.
[13] Shames, I. H., and Dym, C. L., *Energy and Finite Element Methods in Structural Mechanics*, Hemisphere, Washington, D.C., 1985.
[14] *Metallic Materials and Elements for Aerospace Vehicle Structures*, U.S. Department of Defense, MIL-HDBK-5J, Jan. 2003.
[15] Pratt, K. G., and Walker, W. G., "A Revised Gust-Load Formula and Re-Evaluation of V-G Data Taken on Civil Transport Airplanes from 1933–1950," NACA Rept. 1206, 1955.
[16] McCullers, L. A., "Aircraft Configuration Optimization Including Optimized Flight Profiles," *Recent Experiences in Multidisciplinary Analysis and Optimization*, edited by J. Sobieski, NASA CP-2327, April 1984.
[17] Bhatia, M., Kapania, R. K., van Hoek, M., and Haftka, R. T., "Structural Design of a Truss Braced Wing: Potential and Challenges," 50th AIAA/ASME/ASCE/AHS/ASC Structures, Structural Dynamics, and Materials Conference, AIAA Paper 2009-2147, Palm Springs, CA, May 2009.
[18] Blackwell, J., "Numerical Method to Calculate the Induced Drag or Optimal Span Loading for Arbitrary Non-Planar Aircraft," NASA SP-405, May 1976.
[19] Grasmeyer, J., "A Discrete Vortex Method for Calculating the Minimum Induced Drag and Optimum Load Distribution for Aircraft Configurations with Noncoplanar Surfaces," Virginia Polytechnic Inst. and State Univ. Multidisciplinary Analysis and Design Center for Advanced Vehicles, Department of Aerospace and Ocean Engineering, Rept. VPI-AOE-242, Blacksburg, VA, Jan. 1997.
[20] Gur, O., Mason, W. H., and Schetz, J. A., "Full Configuration Drag Prediction," 27th AIAA Applied Aerodynamics Conference, AIAA Paper 2009-4109, San Antonio, TX, June 22–25, 2009.
[21] White, F. M., *Viscous Fluid Flow*, McGraw-Hill, New York, 1974.
[22] Hopkins, E. J., and Inoye, M., "An Evaluation of Theories for Predicting Turbulent Skin Friction and Heat Transfer on Flat Plates at Supersonic and Hypersonic Mach Numbers," *AIAA Journal*, Vol. 9, No. 6, June 1971, pp. 993–1003. doi:10.2514/3.6323
[23] Hopkins, E. J., "Charts for Predicting Turbulent Skin Friction from the Van Driest Method (II)," NASA TN D-6945, Oct. 1972.
[24] Liu, C., "Drag of a Flat Plate with Transition in the Absence of Pressure Gradient," *Journal of Aircraft*, Vol. 9, No. 7, July 1972, pp. 509–510. doi:10.2514/3.59026
[25] Collar, A. R., "A Closed Formula for the Drag of a Flat Plate with Transition in the Absence of a Pressure Gradient," *Journal of the Royal Aeronautical Society*, Vol. 64, Jan. 1960, pp. 38–39.
[26] Cebeci, T., and Bradshaw, P., *Momentum Transfer in Boundary Layers*, McGraw–Hill, New York, 1977.
[27] Braslow, A. L., Bartlett, D. W., Wagner, R. D., and Collier, F. S. Jr., "Applied Aspects of Laminar-Flow Technology," *Viscous Drag Reduction in Turbulent Boundary Layers*, edited by D. M. Bushnell and J. N. Hefner, Vol. 123, Progress in Aeronautics and Astronautics, AIAA, New York, 1990.
[28] Boltz, F. W., Kenyon, G. C., and Allen, C. Q., "Effects of Sweep Angle on the Boundary-Layer Stability Characteristics of an Untapered Wing at Low Speeds," NASA TN D-338, Oct. 1960.
[29] Wagner, R. D., Bartlett, D. W., and Collier, F. S. Jr., "Laminar Flow—The Past, Present, and Prospects," 2nd AIAA Shear Flow Conference, AIAA Paper 1989-0989, Tempe, AZ, March 1989.
[30] Hoerner, S. F., *Fluid Dynamic Drag*, Hoerner Fluid Dynamics, Bakersfield, CA, 1965.
[31] Torenbeek, E., *Synthesis of Subsonic Airplane Design*, Delft University Press, Delft, The Netherlands, and Martinus Nijhoff Publishers, Hague, The Netherlands, 1982.
[32] Jobe, C. E., "Prediction and Verification of Aerodynamic Drag, Part I: Prediction," *Thrust and Drag: Its Prediction and Verification*, edited by C. E. Eugene, Vol. 98, Progress in Astronautics and Aeronautics, AIAA, New York, 1985, Chap. 4.
[33] Shevell, R. S., *Fundamentals of Flight*, Prentice-Hall, Upper Saddle River, NJ, 1989.
[34] Nicolai, M. L., *Fundamentals of Aircraft Design*, METS, Inc., San Jose, CA, 1984.
[35] Raymer, D. P., *Aircraft Design: A Conceptual Approach*, 4th ed., AIAA Education Series, AIAA, Reston, VA, 2006.
[36] Mason, W. H., "Analytic models for technology integration in aircraft design," AHS and ASEE Aircraft Design, Systems, and Operations Conference, AIAA Paper 1990-3262, Dayton, OH, Sept. 1990.
[37] Inger, G. R., "Application of Oswatitsch's Theorem to Supercritical Airfoil Drag Calculation," *Journal of Aircraft*, Vol. 30, No. 3, May–June 1993, pp. 415–416. doi:10.2514/3.46354
[38] Hilton, H. W., *High Speed Aerodynamics*, Longmans, Green and Co., London, 1951.
[39] Malone, B., and Mason, W. H., "Multidisciplinary Optimization in Aircraft Design Using Analytic Technology Models," *Journal of Aircraft*, Vol. 32, No. 2, March–April 1995, pp. 431–438. doi:10.2514/3.46734
[40] Tétrault, P.-A., Schetz, J. A., and Grossman, B., "Numerical Prediction of the Interference Drag of Strut-Surface Intersecting in Transonic Flow," *AIAA Journal*, Vol. 39, No. 5, May 2001, pp. 857–864. doi:10.2514/2.1389
[41] Duggirala, R. K., Roy, C. J., and Schetz, J. A., "Analysis of Interference Drag for Strut-Strut Interaction in Transonic Flow," 47th AIAA Aerospace Sciences Meeting, AIAA Paper 2009-0051, Orlando, FL, Jan. 2009.
[42] Hurel, M., "The Advantages of High Aspect Ratios," *Interavia, Aerospace World : Business and Technology*, Vol. 7, No. 12, 1952, pp. 695–699.
[43] Renzelmann, M. E., "Self-Monitoring Latch Pin Lock for Folding Wing Aircraft," U.S. Patent 5201479, April 1993.
[44] York, P., and Labell, R. W., "Aircraft Wing Weight Build-Up Methodology with Modification for Materials and Construction Techniques," NASA CR-166173, Sept. 1980.
[45] Goldschmied, F. R., "Fuselage Self-Propulsion by Static-Pressure Thrust: Wind-Tunnel Verification," AHS and ASEE Aircraft Design, Systems, and Operations Meeting, AIAA Paper 1987-2935, Saint Louis, MO, Sept. 1987.